Two-Dimensional Electronic Spectroscopy of β-Carotene

Niklas Christensson,[†] Franz Milota,[‡] Alexandra Nemeth,[‡] Jaroslaw Sperling,[‡] Harald F. Kauffmann,[‡,§] Tönu Pullerits,[†] and Jürgen Hauer*[,‡]

Department of Chemical Physics, Lund University, Box 124, SE-21000, Lund, Sweden, Department of Physical Chemistry, University of Vienna, Währingerstr. 42, A-1090 Vienna, Austria, and Ultrafast Dynamics Group, Faculty of Physics, Vienna University of Technology, Wiedner Hauptstrasse 8-10, A-1040, Vienna, Austria

Received: July 13, 2009; Revised Manuscript Received: September 29, 2009

Two-dimensional electronic spectroscopy (2D) has been applied to β-carotene in solution to shine new light on the ultrafast energy dissipation network in carotenoids. The ability of 2D to relieve spectral congestion provides new experimental grounds for resolving the rise of the excited state absorption signal between 18 000 and 19 000 cm^{-1}. In this spectral region, the pump−probe signals from ground state bleach and stimulated emission overlap strongly. Combined modeling of the time-evolution of 2D spectra as well as comparison to published pump−probe data allow us to draw conclusions on both the electronic structure of β-carotene as well as the spectral densities giving rise to the observed optical lineshapes. To account for the experimental observations on all time scales, we need to include a transition in the visible spectral range from the first optically allowed excited state ($S_2 \rightarrow S_{n2}$). We present data from frequency resolved transient grating and pump−probe experiments confirming the importance of this transition. Furthermore, we investigate the role and nature of the S* state, controversially debated in numerous previous studies. On the basis of the analysis of Feynman diagrams, we show that the properties of S*-related signals in $\chi^{(3)}$ techniques like pump−probe and 2D can only be accounted for if S* is an excited electronic state. Against this background, we discuss a new interpretation of pump−deplete−probe and intensity-dependent pump−probe experiments.

1. Introduction

Carotenoids are a family of naturally occurring pigments that are one of the most abundant in nature. All carotenoids share a polyene like motif in their structure (see Figure 1) resulting in a conjugated system of π-electrons that is responsible for many of their optical properties. The biological functions of carotenoids, namely, light harvesting and photoprotection, can be qualitatively understood in terms of their electronic structure.[1] Early studies revealed that the strongly absorbing S_2 state was not the lowest excited state of carotenoids. The lowest excited state, S_1, is located below S_2 in all carotenoids. S_1 is dark with respect to the ground state due to its symmetry but is readily observed via its excited state absorption (ESA) in the visible region.[2] While most of the biological relevance of carotenoids can be understood via the energetic position of the dark S_1 state and the strongly allowed S_2 state, these two states are not enough to account for all experimental investigations of carotenoid photophysics. Besides S_2 and S_1, experiments with ultrashort pulses have indicated that other states are also involved in carotenoid photophysics.[3] Despite the intense experimental efforts including pump−probe,[1,4] fluorescence upconversion,[5,6] transient grating,[7,8] pump−deplete−probe,[9,10] pump degenerate four wave mixing (Pump-DFWM),[11,12] femtosecond stimulated Raman,[13–15] quantum control,[16–18] and photon echo spectroscopy,[19] the details of the electronic structure of carotenoids are still a matter of debate. One particularly interesting result obtained from the pump−probe studies is the shoulder on the high-energy side of the $S_1 \rightarrow S_{n1}$ ESA spectra. This feature has been assigned to the so-called S* state,[20] and its behavior has been thoroughly investigated.[3] The perhaps most striking property of S* can be found in longer carotenoids where the lifetime of S* can be a few times longer than the S_1 lifetime.[9,10] Despite numerous experimental studies, there is no consistent picture about the nature of this state nor its energetic position relative to the ground state. An intensity-dependent pump−probe study in LH2 revealed that S* and S_1 had different intensity dependences and found that S* was a precursor to triplet formation.[21] This observations placed S* as an excited state in the vicinity of S_1. To account for the key experimental observation, that the S* spectral feature was more intense at higher pump intensity, it was postulated that there exists an ESA transition directly from S_2 in the visible spectral region and that the relaxation from this higher lying state preferably populates S*. Due to the additional state and the mechanism for enhancement of the S* spectral feature, the model was named the two-photon model.[21] The authors also elaborated on the inhomoge-

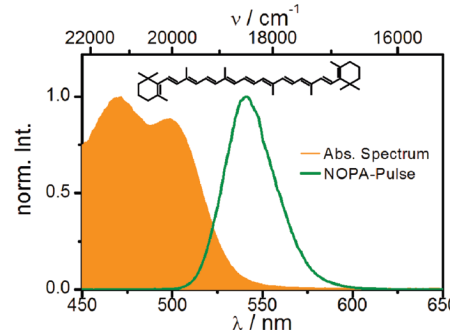

Figure 1. Absorption spectrum of β-carotene dissolved in benzonitrile together with the spectrum of the excitation pulse (green line). Shown on the top is the structure of β-carotene.

* Corresponding author. E-mail: juergen.hauer@univie.ac.at.
[†] Lund University.
[‡] University of Vienna.
[§] Vienna University of Technology.

10.1021/jp906604j
Published on Web 12/02/2009

neous model where S* was the result of ground state conformational disorder. They found however that such a model would require unrealistic differences in the transition dipole moment of the two conformations to explain the data. The different intensity dependence of S_1 and S* was later confirmed by Savolainen et al.[22] in a study of a carotenoid as a part of an artificial light-harvesting system. However, the model these authors suggested was somewhat simpler compared to the two-photon model, involving only S_2, S_1, and a vibrationally hot ground state (hot S_0).

Further studies on the nature of S* showed that the respective spectral signature was strongly suppressed at 77 K.[23] It was proposed that S* was the result of a twisted conformation of S_1 formed in the relaxation from S_2.[23–25] The inhibition of S* at low temperature was argued to be the result of insufficient thermal energy to activate the conformational change in the excited state. This hypothesis as well as the two-photon model was later challenged by an elegant pump−probe experiment involving an additional deplete pulse tailored to remove population from S_2 before the formation of any lower lying excited states.[9,10] These pump−deplete−probe experiments revealed that only the S_1 transient absorption feature was sensitive to the presence of the depletion pulse leading to the conclusion that both S* and S_1 could not be formed from the same precursor state. To explain these results, a hypothesis was put forward where S* was a hot ground state formed by an impulsive stimulated Raman process (ISRS) within the pump pulse.[9,10] The nature of the S* state thus remains elusive, and no single model has been put forward to account for all the experimental observations. For an elaborate and up-to-date review of the experimental efforts in clarifying the nature of S*, we refer the reader to a recent review.[3]

Most of the experimental investigations on carotenoids have been carried out using the pump−probe technique, and we take this experiment as the starting point of our discussion of the 2D experiments employed in this study. A schematic of the pump−probe pulse sequence is illustrated in Figure 2(A). The pump−probe technique belongs to the class of third-order nonlinear optical experiments. Consequently, it requires three light-matter interactions. To meet this criterion, the pump pulse must interact twice (i.e., $-k_1 + k_1$). Phase matching then ensures that the polarization is radiated in the direction of the probe (i.e., $k_s = k_2$). Hence, the probe field heterodynes the signal field, and the real part of the polarization is directly measured. The pump−probe experiment has a built-in weakness in that it derives two of its interactions from the same laser pulse, thereby projecting the third-order nonlinear polarization onto only two independent coordinates, namely, the delay between the pump and probe, t_2, and the frequency of the emitted polarization ν_3. Such reduction leads to incomplete information about the system dynamics and its interaction with the environment. The use of two interactions from one pulse also sets constraints on the temporal and spectral resolution of a pump−probe experiment. The maximum time delay between two interactions coming from the same pulse is roughly given by the pulse duration. The short time between these interactions corresponds to a large uncertainty in frequency. In this way the spectral and temporal resolution of a pump−probe experiment are related via a Fourier transform.[26] It is thus inevitable to sacrifice spectral resolution in the pump when attempting to resolve the fastest processes in a pump−probe experiment.

It is clear that more complete information on the system's third-order polarization can be obtained if the polarization is interrogated in all of its three dimensions. This is done in a 2D

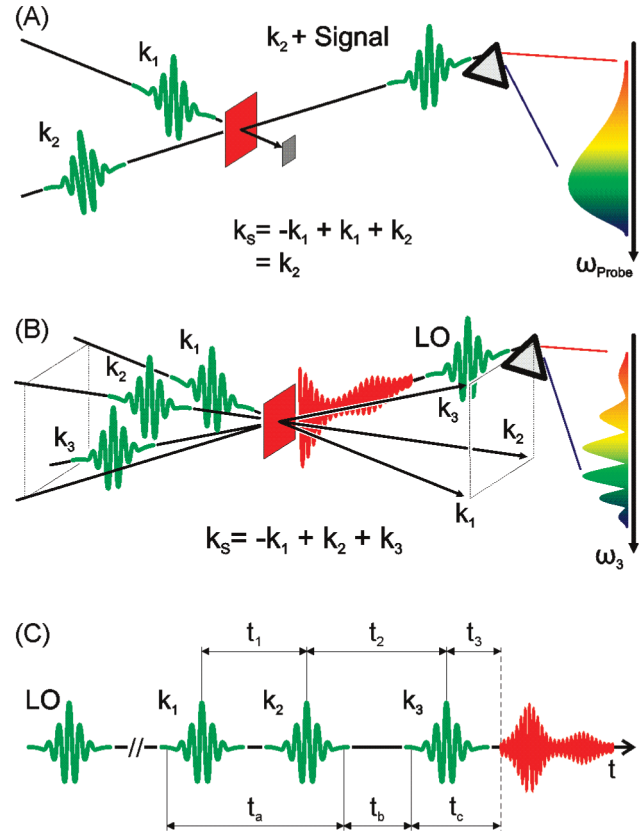

Figure 2. Experimental configurations for the pump−probe (A) and the 2D experiment (B). In the pump−probe sequence (A) only two pulses are involved in the experiments, meaning that two of the light−matter interactions derive from the same laser pulse. Phase matching dictates that the signal radiates in the direction of the probe ensuring heterodyne detection of the signal field. In the 2D sequence (B), all interactions come from different pulses, and the polarization is detected in the phase matched direction $k_s = -k_1 + k_2 + k_3$. To determine the signal field, a local oscillator is spatially overlapped with the signal, and the amplitude and phase of the polarization field are determined via spectral interferometry. Panel (C) shows the definitions of the experimentally controllable time delays t_1, t_2, and t_3 as well as the time delay between the light−matter interactions t_a, t_b, and t_c.

experiment[27,28] where all three interactions stem from different pulses propagating with different wave vectors and have independently controllable delays as shown in Figure 2(B). After interacting with the three different pulses, a signal field is generated in the $-k_1 + k_2 + k_3$ phase matching direction. To obtain the complete information about the signal field and not just its intensity like in standard photon echo experiments,[29] a local oscillator is spatially overlapped with the signal field, and the amplitude and phase of the signal are retrieved by spectral interferometry.[30] The signal field $S(t_1, t_2, \nu_3)$ recorded for different delays between the first two pulses t_1 is then used to calculate the 2D spectrum $S(\nu_1, t_2, \nu_3)$ for specified values of t_2. This step requires a Fourier transformation along t_1,[27,28] implying that this delay has to be controlled with interferometric accuracy to avoid distortions in the Fourier transform.[27,28] Spectral interferometry with a separate local oscillator only determines the 2D spectra up to a constant phase. The correct phase is obtained by adjusting the absolute phase of the 2D spectra until the projection of the real part onto ν_3 matches the spectrally resolved pump−probe signal.[31] The 2D experiment is then repeated for different values of the population time t_2 to fully exploit the three-dimensional nature of the third-order polarization.

The ability to control the delay between the first two pulses (t_1) has implications for the spectral and temporal resolution in a 2D experiment. If the delay between the first two interactions can be controlled, it can be extended thereby increasing the spectral resolution. The temporal resolution is still determined by the ability to define the time of a specific interaction, i.e., by the pulse duration. Hence, for a 2D experiment the usual Fourier relation between spectral and temporal resolution does not apply, and the spectral resolution can be improved without sacrificing temporal resolution. The increase in spectral resolution compared to pump−probe becomes evident when considering that pump−probe spectra are the projection of 2D spectra onto ν_3. As a consequence of the higher spectral resolution and higher dimensionality, 2D spectra are less congested. This property can be used to circumvent inhomogeneous broadening in the ground state, but the same argument applies to spectral congestion due to multiple electronic transitions. The ability to control the first interaction period has additional benefits. Following the coherence evolution during t_1 explicitly, it becomes possible to correlate it to the coherence evolution during t_3. The loss of correlation with increasing population time t_2 gives a measure of decoherence of the system, thereby allowing the study of the interaction of electronic and nuclear degrees of freedom.[29,32,33]

With full control of all time delays and the detection of the signal field, 2D constitutes the most complete third-order experiment. In fact, any other third-order signal can be calculated from 2D spectra via the projection slice theorem.[28] However, in its standard implementation 2D has one limitation besides the considerably more complex experimental setup.[34,35] Typically, a 2D experiment employs degenerate pulses for all interactions, and even though pulses spanning $\sim$3000 cm^{-1} are available, this leads to finite bandwidth effects in the experiment. The finite bandwidth leads to a spectral selection of the polarization and incomplete information about the evolution of the coherences during t_1 and t_3. To simultaneously cover the ground state bleach (GSB) as well as the ESA of carotenoids, a degenerate 2D experiment would need a 150 nm broad pulse centered at 525 nm, corresponding to transform limited pulses of 3 fs duration. This is clearly difficult to achieve experimentally. It is therefore very fruitful to use 2D for the spectral regions where the dynamics is fast and the spectra are congested and complement with broadband pump−probe to obtain the induced polarization as a function of ν_3 for all electronic transitions of interest.

In this article, we report on 2D electronic spectroscopy of β-carotene in solution. Figure 1 shows the linear absorption spectra of β-carotene as well as the spectrum of the laser pulses used in the experiments. Unlike most 2D experiments, the laser pulses are detuned to the far red edge of the linear absorption spectra. This maximizes the sensitivity of the experiment to a spectral region that is notoriously congested with transitions from GSB, stimulated emission (SE), and ESA from both S_1 and S*. To aid interpretation of the experimental results, simulations of both the time evolution of the 2D spectra as well as the pump−probe spectra and dynamics are carried out.

2. Experimental Procedure

Excitation of the sample was accomplished by a home-built noncollinear optical parametric amplifier (NOPA)[36] pumped by a regenerative titanium−sapphire amplifier system (RegA 9050, Coherent Inc.) at 200 kHz repetition rate. The pulses had a central wavelength of 545 nm (18 350 cm^{-1}) with a bandwidth of 1280 cm^{-1} and a duration of 16 fs fwhm, determined by intensity autocorrelation. The pulses were attenuated by a neutral density filter to yield 8.5 nJ per excitation pulse at the sample. This corresponds to a fluence of $4.0 \cdot 10^{14}$ photons/cm^2 per pulse or 0.5% of excited molecules in the focal volume. The 2D experiment relies on a passively phase stabilized setup with a transmission grating[31,34,35] and has a temporal resolution of 5.3 as for t_1 and 0.67 fs for t_2. A detailed description can be found in Nemeth et al.[37] and Milota et al.[38] The time-zero points for the scanned time delays (t_1 and t_2) were determined by spectral interferometry between the respective excitation pulses.[31] The obtained interferograms in a 2D measurement (see Figure 2B) showed no phase drift during the course of measurements performed during one day. Sample handling was accomplished by a wire-guided drop jet[39] with a flow rate of 20 mL/min and a film thickness of approximately 200 μm. β-Carotene was purchased from Sigma-Aldrich and used as received. For the solutions, 20 mg of the sample was dissolved in 100 mL of benzonitrile (Sigma-Aldrich, spectrophotometric grade). The sample solution was filtrated before use to remove insoluble residues. All measurements were performed under ambient temperatures (295 K).

3. Experimental Results

The real parts of the measured 2D spectra of β-carotene in benzonitrile are shown in Figure 3. At $t_2 = 0$ fs, some qualitative features of the signal can be directly seen. Except for a weak negative (ESA) band, the signal is mostly positive (GSB) with one large peak elongated along the diagonal. The GSB/SE peak positioned along the diagonal shows a pronounced elongation indicative of spectral inhomogeneity. At lower emission frequencies (i.e., at $[\nu_1; \nu_3] = [-19\,150; 17\,650]$), there is a vibrational cross peak corresponding to the ground state wave packet prepared by the first two interactions via a ISRS process. This feature shows an oscillating behavior with respect to t_2, and we identify it as the 1150 cm^{-1} C−C vibrational mode.[40] The 2D spectra at $t_2 = 40$ fs and $t_2 = 60$ fs clearly reveal the power of 2D when it comes to reducing spectral congestion. We note that the pump−probe spectrum is the projection of the real part of the 2D spectra onto ν_3. The 2D spectra reveal a significant overlap between GSB/SE and excited state absorption in the $\nu_3 = 18\,000-19\,000$ cm^{-1} range. For instance, at $t_2 = 40$ fs the pump−probe signal below $\nu_3 = 18\,000$ cm^{-1} is negative, but the 2D spectra clearly reveal the presence of the vibrational wave packet.

The experimental result presented here gives no indication of a significant ultrafast Stokes shift for β-carotene in benzonitrile. If an ultrafast Stokes shift was present, the positive feature would elongate along ν_3 and at the same time become more round.[37,41] Rather, the GSB signal maintains its shape during the first 60 fs showing little indication of fast spectral diffusion. The initially prepared S_2 state decays to populate S_1 on a 150 fs time scale.[42] The negative feature below $\nu_3 = 18\,000$ cm^{-1} consequently gains in strength as S_1 is populated via relaxation from S_2. As the ESA signal rises between $t_2 = 40$ fs and $t_2 = 400$ fs, it pushes up the GSB signal to higher ν_3. This blue shift of the signal on a 100 fs time scale appears to be too fast to be assigned to vibrational relaxation in S_1, a process that has been shown to take place with a 200−400 fs time constant.[11−14,43] The rise of the ESA signal also leads to a change of the nodal line[33] of the GSB component. At $t_2 = 400$ fs, the ESA significantly distorts the shape of the GSB signal, making the nodal line between GSB and excited state absorption almost vertical. This does not reflect dephasing of the GSB transition since the GSB still has a significant elipticity.[37,41] Rather, we

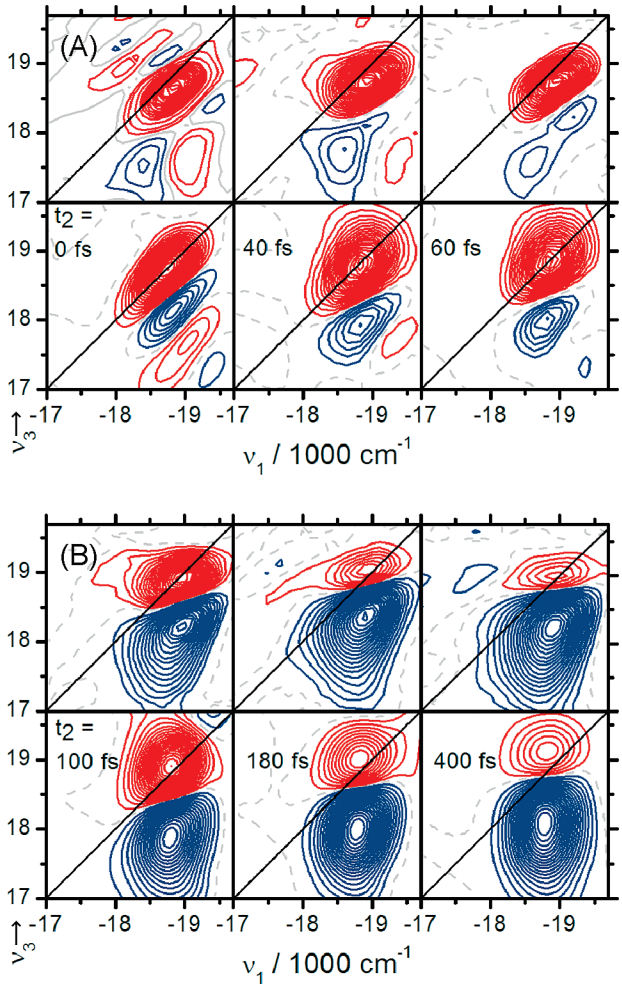

Figure 3. Real part of the 2D spectra of β-carotene in benzonitrile for different population times t_2 indicated in each panel. For both (A) and (B), showing early and later times, respectively, the top row shows the experimental results, while the lower row depicts simulations discussed in the text. The contour lines are drawn based on a linear scale in ± 5% steps. All spectra are normalized to their maximum absolute value. Red (blue) lines indicate positive (negative) signals. Nodal lines (lines of zero intensity) are dashed.

interpret the blue shift and the change of the nodal line as a result of the change of the strength of the positive and negative components due to population dynamics. For a more detailed description of the dynamics, it is necessary to resort to numerical simulations.

4. Discussion

The following section is devoted to motivate and discuss the model and approximations underlying the simulation results in Figure 3. In section 4.1, we outline the energy level structure and population dynamics of the model. In sections 4.2 and 4.3, we explain the two cornerstones of the proposed energy level scheme in detail, namely, the $S_2 \rightarrow S_{n2}$ transition and the specification of S* as an electronically excited state. In section 4.4, we discuss higher-order processes including $\chi^{(5)}$-experiments like Pump-DFWM. Section 4.5 deals with model calculations of broadband pump−probe spectra and compares them to previously reported results. In section 4.6, we discuss the effect of vibrational cooling in S_1, while section 4.7 explains the neglect of possible intermediate states between S_2 and S_1. Besides the population dynamics described via rate equations defined by the energy level structure, the model also includes

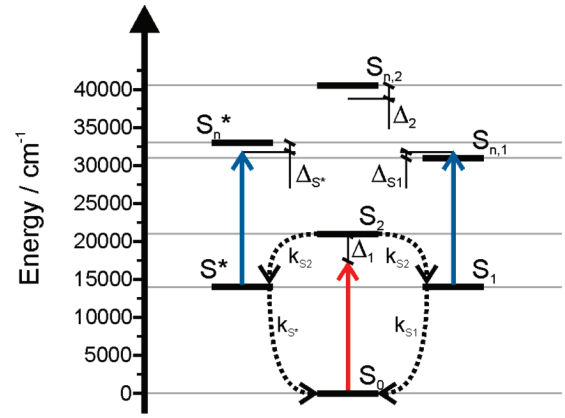

Figure 4. Energy level structure of the model used in the simulations. In accordance with the 2D-data plots in Figure 3, the ESA transitions are indicated by blue arrows, while GSB and SE are shown as a red arrow. The population decay channels with the corresponding rates (k_{S2}, k_{S1}, k_{S*}) as well as the detuning (Δ_1, Δ_2, Δ_{S1}, Δ_{S*}) of each state from the laser central frequency are also indicated. Vibrationally hot S_1 as a distinct state is omitted since it is not probed in the limited excitation bandwidth of the experiment (see section 4.6 for further details).

system bath interactions. This point and the respective response functions as well as spectral densities for the transitions included in the model are discussed in section 4.8. The discussion of pump−deplete−probe experiments in section 4.9 will finalize our discussion, leading to a refined model for β-carotene's energy dissipation network.

4.1. Model of β-Carotene's Optical Response. The experiments reported here focus on the most congested spectral region of the carotenoid optical response, in which GSB, SE, $S_1 \rightarrow S_{n1}$ (ESA), and $S^* \rightarrow S_n^*$ (ESA) plus possible additional transitions contribute to the spectroscopic signals. To go beyond the qualitative discussion of the experimental results, the spectral properties of all transitions, their mutual overlaps, as well as pulse overlap effects need to be considered. As a starting point for our analysis, we adopt the model by Christensson et al.[19] for the third-order optical response of carotenoids. It incorporates both the system bath interaction as well as population dynamics. Pulse overlap effects and spectral selection are taken into account by convoluting the response functions of the system with the finite electric fields used in the experiments. The large bandwidth of the pulses used in the experiments means that the vibrational modes of the carotenoid need to be taken into account in the simulations. We find that including two vibrational modes of 1150 and 1520 cm^{-1} is sufficient to account for the linear absorption spectra (not shown) as well as the 2D experiments. To incorporate any effects related to chirp of the excitation pulses, we characterized the pulses via SH-FROG prior to every experiment and used the retrieved phase for the model calculations.

For the energy level structure of β-carotene, we employ a model including S_0, S_1, S_2, as well as the higher lying S_{n2}.[19] In addition, we place S* as an excited electronic state. Figure 4 shows the relevant energy levels and the corresponding electronic transitions of the model. For population times shorter than the S_2 lifetime, the signal polarization will exhibit contributions from GSB, SE, and $S_2 \rightarrow S_{n2}$ ESA. Due to population relaxation, all pathways that are in S_2 population during t_2 decay with a 150 fs time constant. We have assumed a branched decay from S_2 implying that S_1 and S* rise with the same time constant. If the rise times of the two states were different, the shape of the negative feature in the 2D spectra would change between $t_2 =$ 100 fs and $t_2 =$ 400 fs. From Figure 3, it is evident that the

TABLE 1: Energies of the Electronic Transitions Involved in the Model[a]

	$\nu_{vertical}$ (cm^{-1})	ν_{0-0} (cm^{-1})	$\|\mu\|$
$S_2 \rightarrow S_{n2}$	18700	18330	0.85
$S_0 \rightarrow S_2$	21150	18950	1
$S^* \rightarrow S_n^*$	18250	16945	0.63
$S_1 \rightarrow S_{n1}$	17350	16045	1.12

[a] The first column gives the vertical transition energy relative to the ground state while the second gives the energy of the pure electronic transition. The last column gives the transition dipole moment of the specific transition normalized to the $S_0 \rightarrow S_2$ transition.

shape of the ESA does not alter appreciably during this time interval, supporting our assumption of a similar rise time of the S_1 and S* state. Furthermore, the population relaxation is assumed to be incoherent, meaning that the transition frequency fluctuations during t_1 and t_3 are uncorrelated[19,44] (see section 4.7). As discussed in the Introduction, experiments have shown that the relaxation rates for S_1 and S* are different. Here we have set the lifetimes of the S_1 and S* states to 9 and 10 ps, respectively. The energy of the $S^* \rightarrow S_n^*$ transition is higher than the $S_1 \rightarrow S_{n1}$ transition, and in our simulations we set the difference to 900 cm^{-1}. Neither 2D nor pump−probe can determine if the difference in the transition energy has its origin in a shift of S* or the corresponding S_n* level. However, in light of the proposed origin of S* as a conformation (see section 4.9), we suggest that the energy of S* should not be too different from S_1 indicating that the shift mainly affects the S_n* level. The transition energies and the corresponding transition dipole moments are given in Table 1, and the simulations are shown in the lower panel of Figure 3.

4.2. Transitions Originating from S_2. Previous studies of the initial dynamics in carotenoids have indicated the presence of excited state absorption directly from S_2. This conclusion was reached from fitting of intensity-dependent pump−probe[21] and simulations of the integrated[7,8] or frequency resolved transient grating signal (FRTG).[19] We can directly observe indications of a transition from S_2 by inspecting the frequency resolved transient grating signal shown in Figure 5(A). The signal has its maximum for $t_2 < 0$ fs, which cannot occur in a two-level system with finite rephasing capacity.[29] We point out that the solvent signal (not shown) is peaked at $t_2 = 0$ fs with a tail to longer times. To account for the FRTG peaking at $t_2 <$ 0 fs, an ESA transition directly from S_2 is necessary.[19]

The FRTG signal shown in Figure 5 measures the intensity of the emitted field, thereby combining the information from the real and imaginary part of the signal field. This is significant since the integrated transient grating signals have shown oscillations corresponding to solvent modes.[8,11,45] As these modes are excited off-resonantly, they should only be present in the imaginary part of the polarization. Heterodyne transient grating experiments have further shown that the influence of the solvent on the signal in the pulse overlap is significant for homodyne experiments.[46] To avoid the complication of the solvent signal and signals belonging to the imaginary part of the polarization, we restrict our analysis to signals involving the real part of the signal field. We focus here on the pump−probe signal at $t_2 = 0$ fs to investigate the presence of the $S_2 \rightarrow S_{n2}$ transition in β-carotene. Figure 5(B) shows simulations with and without the $S_2 \rightarrow S_{n2}$ transition together with the measured pump−probe signal. The simulations without the $S_2 \rightarrow S_{n2}$ transition produce a pump−probe spectrum showing little resemblance with the experimental results, while the simulations

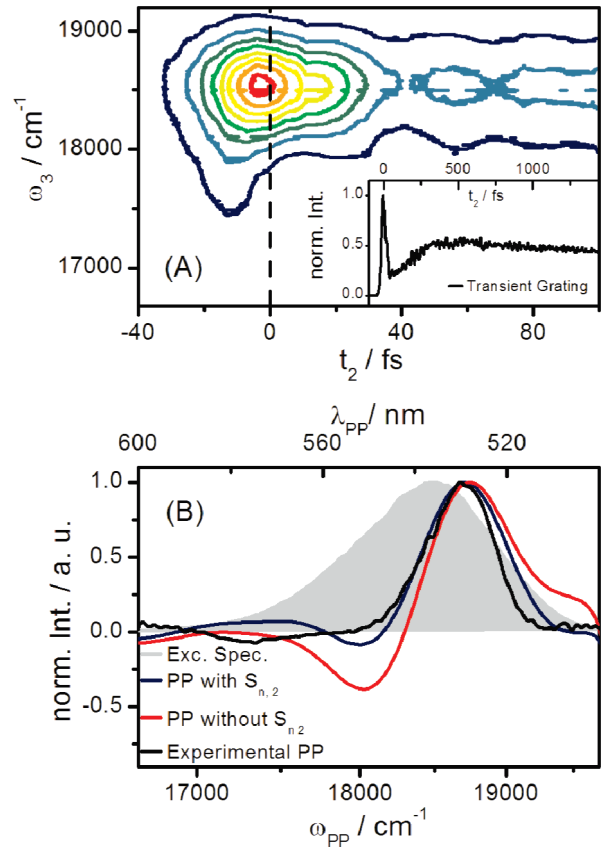

Figure 5. (A) Frequency resolved transient grating signal for β-carotene in benzonitrile. Contour lines are drawn based on a linear scale in 10% steps. The inset shows the integrated transient grating signal that rises for longer t_2 times due to population relaxation to the S_1/S* states. (B) Experimental (black line) degenerate pump−probe spectra at $t_2 = 0$ fs, pumped and probed with the gray-shaded pulse. Also shown is the model including ESA from S_2 (blue line) as well as the same model with the ESA omitted (red line).

including $S_2 \rightarrow S_{n2}$ can account for the general features of the experimental pump−probe spectra.

The $S_2 \rightarrow S_{n2}$ transition in our model should not be confused with previous assignments of ESA from S_2.[47−49] Cerullo et al.[47] assigned a short-lived positive feature covering the entire visible spectral range in the pump−probe spectra to ESA from S_2. This spectral feature was later shown to be related to the double coherence pathways accessible in a three-level system.[48] In the three-level system discussed by Kosumi et al.,[48] the ESA transition from S_2 was located in the near-infrared (NIR) region, and it becomes accessible due to the broadband probe. While we also enlist a three-level system to account for the dynamics, we stress that the $S_2 \rightarrow S_{n2}$ transition has to be located in the visible spectral region to be accessed by the finite bandwidth of our pulses. The $S_2 \rightarrow S_{n2}$ transition proposed here is different from the S_2 ESA transition in the NIR discussed by Kosumi et al.[48] and measured by Zhang et al.[49] We thus conclude that there must be more than one excited state absorption transition originating from the S_2 state.

4.3. S* State. From the time-evolution of the 2D spectra, it is clear that the rise of the negative feature requires at least the inclusion of the $S_1 \rightarrow S_{n1}$ transition. To address the possible need for more states (i.e., S*), we need to examine the influence of the system bath interaction on each transition. This holds particularly true for the vibrational modes coupling to the $S_1 \rightarrow S_{n1}$ transition. Previous experimental investigations including excited state transient grating[11,12,43] and time-resolved Raman

spectroscopy[13–15] have shown vibrational modes with characteristic frequencies of S_1. However, from such experiments it is not clear how strongly the modes couple to the electronic transition. Strong coupling between vibrational modes and the $S_1 \rightarrow S_{n1}$ transition could be responsible for the shoulder of the ESA spectra attributed to S*. We find that a model neglecting S* and having only strong electron vibration coupling of the $S_1 \rightarrow S_{n1}$ transition shows a strong negative feature above $\nu_3 = 19\,500\ \mathrm{cm}^{-1}$ in the 2D spectra, something not seen in the experiments. Furthermore, if the shoulder of the transient absorption spectra was caused by a strong vibrational mode it would have the same lifetime as the main peak since both transitions would share a common ground state. This is in contrast to experimental results where the S* lifetime is typically longer than the corresponding S_1 lifetime.[3,9,10] We must therefore conclude that the spectroscopic feature assigned to S* is the result of a separate electronic state. This also implies that the Huang−Rhys factors of the vibrational modes coupled to the $S_1 \rightarrow S_{n1}$ transition must be sufficiently weak not to cause any significant modulation of the relaxed $S_1 \rightarrow S_{n1}$ transient absorption spectra or any appreciable signal above $\nu_3 = 19\,500\ \mathrm{cm}^{-1}$ in the 2D spectra.

Having confirmed that it is not possible to simultaneously account for the 2D and pump−probe spectra and dynamics assuming only strong electron-vibration coupling for $S_1 \rightarrow S_{n1}$ transition, we must add an additional state in our simulations. We note that this state must have a lifetime comparable to the S_1 lifetime. Further discussion of possible short-lived intermediate states is given in section 4.6. The addition of a new state opens extra pathways that require a response function and a corresponding Feynman diagram.[32] In the literature, there are two different ways of positioning S* responsible for the shoulder of the transient absorption spectra. Either it is placed as an excited state in the vicinity of S_1 and populated via relaxation from S_2[21,23,25,50] or it is positioned as a hot ground state and populated via ISRS.[9,10] In Figure 6, we show the Feynman diagrams for the two different energy level positions, as detected in a $\chi^{(3)}$ pump−probe experiment. For brevity we only show the diagram corresponding to the pulse ordering 1−2−3 relevant for long population times t_2. The hot ground state model produces two distinct pathways, while the excited state model only generates a single pathway. The first pathway for the hot ground state model evolves on S_2 during t_2 and will decay with the S_2 lifetime. The second pathway propagates in an electronic coherence during t_2, and it would be surprising if this electronic coherence has picosecond dephasing time. Nonetheless, the most significant difference between the models is the numbers of interactions with the bra side of the diagram (the right side). The Feynman diagram for the excited state model has an odd number of interactions with the bra side giving this pathway a negative sign[32] indicative of ESA. At the same time, we must conclude that the hot ground state model only leads to positive contributions (GSB). If we were to introduce S* as a hot ground state we would see a rising positive (negative) component in the 2D spectra (pump−probe). We conclude this section by noting that if S_2 relaxes to a hot ground state during t_2 one can construct a pathway with the correct sign. It is then equivalent to the excited state S* diagram. We find that this is unlikely since it implies an $S_2 \rightarrow S_0$ internal conversion rate that is comparable to the $S_2 \rightarrow S_1$ relaxation rate.

4.4. $\chi^{(5)}$-Experiments. While we do not see any indication of a hot ground state in $\chi^{(3)}$-methods like 2D, it has been shown to contribute to higher-order signals like pump-DFWM.[11] In this $\chi^{(5)}$-technique, a pump pulse precedes the DFWM sequence. This will prepare the system in an excited state prior to the interaction with the DFWM sequence. In this case, the transition to the higher vibrational levels of the ground state is favored due to the red-shifted pulses in the DFWM sequence, and under these conditions the hot ground state can dominate the signal.[11] However, this result from a fifth-order technique does not resolve the sign problem for third-order experiments like pump−probe or 2D.

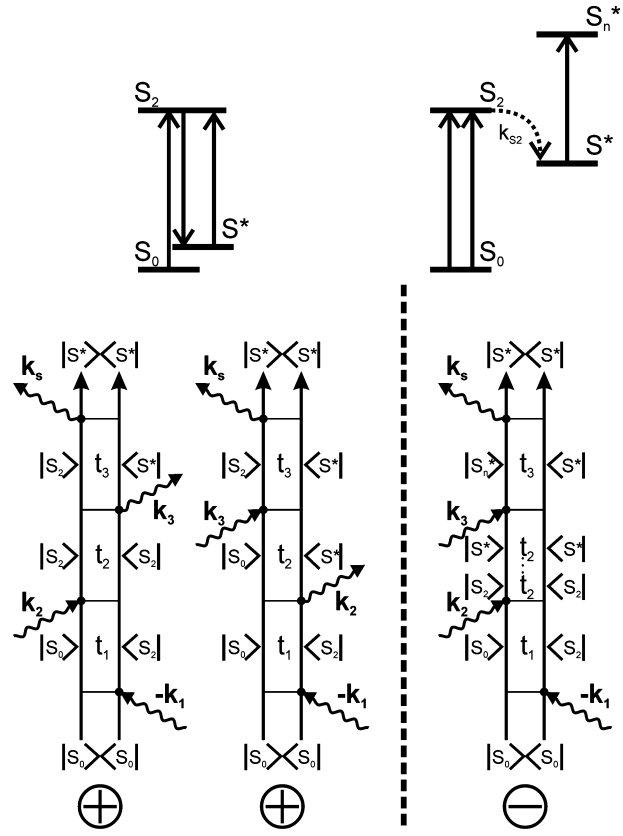

Figure 6. Feynman diagrams for the hot ground state model (left) and the excited state S* model (right) for pulse ordering 1−2−3. The energy level structures of the two models are shown on top of the corresponding diagrams.

The $S_0 \rightarrow S_2$ transition of carotenoids is one of the strongest transitions found in nature, and in principle higher-order processes may take place even at moderate excitation densities. If one allows for a fifth-order interaction in pump−probe (two-photon pump and linear probe), it is possible to create a population in the hot ground state during t_2 and subsequently observe ESA from this transiently populated state. From the recent intensity-dependent pump−probe study by Savolainen et al.,[22] one can estimate at what intensity such fifth-order processes start to contribute. The intensity-dependent experiments revealed that the saturation dynamics of the S_1 transient absorption feature could be described by a single exponential process, with a saturation energy of 410 nJ per pulse, corresponding to a fluence of $2.75 \cdot 10^{15}$ photons/cm^2 per pulse. Expanding the exponential in a Taylor series, one finds that the ratio of quadratic to linear terms scales as the inverse of twice the saturation fluence. With the saturation fluence given above, this means that the quadratic term has an amplitude of less than 10% of the linear term at fluences below $5.5 \cdot 10^{14}$ photons/cm^2 per pulse. Quadratic pump energy dependence suggests a fifth-order pump−probe process. This estimation shows that under the excitation conditions employed in this study ($4.0 \cdot 10^{14}$ photons/cm^2 per pulse or 0.5% excitation probability) the fifth-

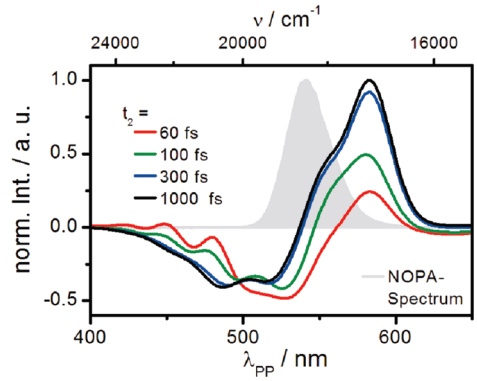

Figure 7. Simulated broadband pump−probe spectra. Both pump and probe are transform-limited with Gaussian shaped envelopes with durations discussed in the text. The pump pulses were centered at 545 nm. The spectra correspond to $t_2 = 60$ fs (red line), $t_2 = 100$ fs (green line), $t_2 = 300$ fs (blue line), and $t_2 = 1000$ fs (black line). The gray-shaded spectrum was used in all 2D measurements.

order process involving the hot ground state is too weak to account for the observed amplitude of S*.

4.5. Model Calculation of Broadband Pump−Probe Spectra. Due to the finite bandwidth of the pulses used in the experiments, the 2D spectra in Figure 3 cannot display the full response of the polarization along ν_3. To put our model into context of the most common experiments, we carried out simulations of the broadband pump−probe spectra. For this calculation, we replaced the last pulse in the sequence with a 2.35 fs transform limited Gaussian pulse (fwhm), while the pump pulse had the same properties as the ones used in the 2D experiments. Figure 7 shows the calculated pump−probe spectra with the model used to describe the 2D data. At short delay times, the pump−probe spectra show intricate behavior due to the coherent contributions introduced by the short probe approximation. However, outside the pulse overlap (i.e., $t_2 >$ 40 fs) one can clearly identify the GSB (520 nm), the S_1 (580 nm), and the S* (550 nm) spectral features. A direct comparison with published pump−probe data is not possible since the spectra depend on the spectral position of the pump pulse as well as its duration. For instance, shifting the excitation pulses 1500 cm^{-1} to the blue (i.e., from 18 350 to 19 850 cm^{-1}), we observe a 10% increase of the S* feature at $t_2 = 1$ ps accompanied by an alternation of the dynamics in the spectral region of S*. This effect is present already in our simple kinetic model and is the result of changes in the ground state wave packet and the overlap of GSB and ESA. To make quantitative comparison with pump−probe spectra, one would need to consider temporal properties of the pump and probe pulses as well as the spectral position of the former. With these reservations in mind we still argue that the similarity between the simulations and published pump−probe data allow us to draw some general conclusions. Inspecting the simulated pump−probe spectra with the most red-shifted pump pulses (i.e., the same as in the 2D experiments) we find a seemingly faster rise of S* compared to S_1. While the rise of S_1 follows a single exponential rise with a 150 fs time constant, S* shows an additional fast rise component. We point out that we observe these phenomena despite the fact that in our model the two states gain population at the same rate. In the 2D spectra (both experimental and simulated) we can see that the ESA contribution containing both S_1 and S* rise with the same time constant. The fast rise constant of S* seen in pump−probe[9] could thus be due to the overlap between a ground state vibrational wave packet and the rise of S*. In the 2D spectra, however, the spectral congestion is partly lifted, and we can observe that the rises for S* and S_1 are very similar.

On one feature, the simulations disagree with the reported experimental pump−probe results. In experiments, the $S_1 \rightarrow S_{n1}$ signal has a component on the red edge of the $S_1 \rightarrow S_{n1}$ peak that decays with a few hundred femtoseconds time constant. This signal has been assigned to signals from a hot S_1.[23,42,51] This assignment was later strengthened by transient grating measurements directly in S_1[11,12,43] as well as time-resolved Raman measurements[13,14] showing vibrational dephasing on a 200−400 fs time scale in S_1. In our description, we have assumed that the relaxation from S_2 populates a thermally equilibrated S_1/S*. The lack of signal to the red of the $S_1 \rightarrow S_{n1}$ transient absorption peak in the simulations is related to the neglect of vibrational relaxation in S_1 in our model. The influence of vibrational relaxation in S_1 on the present 2D experiment will be discussed in the following section.

4.6. Influence of Vibrational Relaxation in S_1 on the 2D Spectra. At first glance, it may seem as if a hot S_1 will not have any impact on our 2D experiment since the spectral feature assigned to the hot S_1 in pump−probe is outside the bandwidth of our laser pulses as can be seen in Figure 7. However, the shoulder on the red side of the $S_1 \rightarrow S_{n1}$ ESA must originate in a Stokes process. This process will be accompanied by an anti-Stokes process at higher energy. Since the anti-Stokes component is shifted by twice the vibrational energy ($\sim$+3000 cm^{-1}), it will be in resonance with the laser pulses used in the experiment. To estimate the magnitude of the anti-Stokes component, we need to consider the vibrational modes in more detail. The coupling of a vibrational mode to the electronic transition is given by the product of the Huang−Rhys factor[32] S_j, the frequency ν_j, and the occupation number of the particular mode $n(\nu_j)$ and is given in eq 1.

$$C_j(\nu) = S_j \cdot \nu_j \cdot \{(n(\nu_j) + 1)\delta(\nu - \nu_j) + (n(-\nu_j))\delta(\nu + \nu_j)\} \quad (1)$$

The first term in the brackets corresponds to the Stokes component, while the second corresponds to the anti-Stokes component. In thermal equilibrium, $n(\nu_j)$ is given by the boson distribution, and the ratio of Stokes to anti-Stokes components is given by the Boltzmann factor. However, in hot S_1 the vibrational modes are not occupied according to equilibrium statistics. Equation 1 shows that raising the occupation number $n(\nu_j)$ leads to an equal increase of both Stokes and anti-Stokes components. This makes it straightforward to estimate the magnitude of the anti-Stokes component via its Stokes counterpart, which is readily observed in pump−probe spectra. From published pump−probe data[42] we estimate that the anti-Stokes component has a maximum contribution of 20% of the maximum $S_1 \rightarrow S_{n1}$ signal.

The estimation of the magnitude of the influence of hot S_1 on the 2D spectra reinforces our statement (section 4.3) that vibrational relaxation is not the origin of the blue shift of the GSB component on $\sim$100 fs time scale. We note that a blue shift of the ESA transition with a magnitude similar to that in the experiment is present in our model (Figure 3) where no vibrational relaxation is present. In our model, the blue shift is related to the change of the overlap of positive and negative features due to population relaxation. To interpret the evolution of the 2D spectra, this change of the overlap between ESA from S_1/S*, GSB/SE, and ground state wave packets is more important than the nonequilibrium vibrational dynamics in S_1.

4.7. Intermediate States. The model shown in Figure 4 treats the relaxation from S_2 to S_1/S* without the involvement of

intermediate states.[52–54] Furthermore, it also does not include any strong vibrational coupling between S_2 and S_1.[55] We find no signatures of any of these processes in the experimental 2D spectra. The agreement between simulations based on a model neglecting such processes and the experiment further strengthens the conclusion that no intermediate states or strong vibronic coupling is necessary to account for the dynamics.

Previous investigations[52–54] have shown that the $S_2 \rightarrow S_1$ relaxation rate does not follow a band gap law, indicating that the weak nonadiabatic coupling description[56,57] is not adequate. These authors pointed to the possibility of intermediate states as the origin of the discrepancy. Christensson et al.[19] argued by analyzing the system bath interaction of carotenoids with similar S_1 energies that the trend in the strength of the system bath interaction was opposite to that of the S_2 decay rate. As the strength of the coupling and the rate are proportional for weak nonadiabatic coupling, they suggested that the relaxation step involves the passage through a conical intersection where a larger coupling to nuclear motions slows down the dynamics. In light of the high rates for the $S_2 \rightarrow S_1$ relaxation, it seems reasonable to assume that the relaxation involves a conical intersection.[58,59] The model considered here assumes that S_1 and S_2 have weakly coupled potential energy surfaces for all nuclear modes that are optically relevant, but there may be directions on the potential energy surface where the coupling between S_1 and S_2 is strong leading to a conical intersection. In such a case, the imprint of the conical intersection on the dynamics as seen by optical experiments is expected to be rather weak.

4.8. System Bath Interaction. One of the strengths of a photon echo experiment is its ability to correlate the frequency fluctuations of a system during t_1 and t_3. The loss of correlation of the frequency fluctuations between these time intervals is a measure of the loss of memory in the system.[32,33,37,41] The analysis of the t_2 evolution of the 2D spectra thus supplies information about both the electronic structure and the system bath interaction of the participating transitions. Unfortunately, the complicated interference between ESA and GSB/SE transitions in the 2D spectra makes it difficult to determine the frequency fluctuations for the GSB. Here we have restricted ourselves to a spectral density comprised of two vibrational modes with frequencies 1150 and 1520 cm^{-1} together with lower frequency overdamped modes. The overdamped modes of the spectral density were described with two fast (40 fs Gaussian and 150 fs exponential) components and a slower (20 ps) exponential component. The reorganization energy of the modes of the $S_0 \rightarrow S_2$ spectral density was set to reproduce the linear absorption spectrum. Despite the uncertainty about the spectral diffusion process due to the population dynamics, we can conclude that both slow and fast overdamped modes are required to account for the dynamics. Furthermore, we can directly conclude from the experimental data that no large Stokes shift is present on the sub 100 fs time scale. In a recent study,[19] it was found that the magnitude of the ultrafast Stokes shift was dependent on the functional groups attached to the conjugated backbone. Given the lack of such functional groups in β-carotene, it is not surprising that the reorganization energy of the fastest modes is rather low. However, the structure of the carotenoid will affect other parts of the spectral density. The presence of β-ionone rings in β-carotene will result in a significant contribution of slow modes to the spectral density.[19,60] In our model the slow exponential component is set to 20 ps, but the time scale of this process is difficult to determine given the limited range of population times probed in the experiments. However, we can conclude that about 400 cm^{-1} reorganization energy has to relax slower than the time scale of the experiments reported here if we are to account for both the 2D spectra as well as the linear absorption spectrum.

Besides the spectral density of the $S_0 \rightarrow S_2$ transition, the experiment is sensitive to the correlation function of the $S_1 \rightarrow S_{n1}$ and $S^* \rightarrow S_n^*$ transitions. In the present system, both ESA pathways involve population relaxation from the S_2 state during the population time t_2. We have assumed that the relaxation is incoherent meaning that the population relaxation destroys the frequency memory, and the frequency fluctuations during the first and third time period become uncorrelated.[44] The observation that it is not possible to transfer a wave packet created in S_2 to a vibrational coherence in S_1[12,17] justifies this approximation. As a consequence of the uncorrelated coherence dynamics during t_1 and t_3 for the pathways involving $S_1 \rightarrow S_{n1}$ and $S^* \rightarrow S_n^*$ transitions, it is also difficult to determine the corresponding spectral densities. In fact, if one assumes that the correlation of the frequency fluctuation is completely lost in the relaxation step, the 2D spectra of the ESA transitions are independent of t_2 and reflect the linear absorption spectra along ν_3.[19,44] Thus, determining the correlation function of the $S_1 \rightarrow S_{n1}$ and $S^* \rightarrow S_n^*$ transitions from the present experiment is just as unique as determining the spectral density for the $S_0 \rightarrow S_2$ transition from the linear absorption spectra alone. It is well-known that such a procedure cannot unambiguously determine the spectral density for the GSB.[32] Despite these limitations a few clear points can be made about the spectral densities for the ESA transitions. As we have discussed above, the coupling of the vibrational modes in S_1 has to be significantly weaker compared to the coupling of the modes to the $S_0 \rightarrow S_2$ transition. Also the narrow $S_1 \rightarrow S_{n1}$ spectrum[42,55] shows that the coupling to the overdamped modes has to be weaker compared to the $S_0 \rightarrow S_2$ spectral density. We expect that the time scales of the correlation functions are rather similar, and we have used the same time scales for all correlation functions. For the simulations we employed a spectral density for the $S_1 \rightarrow S_{n1}$ transition that had $\sim$20% of the coupling to vibrational modes compared to the ground state spectral density. Since femtosecond-Raman experiments[13,14] have shown that the intensity of the S_1 specific mode at 1820 cm^{-1} has similar magnitude as the 1520 cm^{-1} mode, we included this mode into the vibrational part of the spectral density for the $S_1 \rightarrow S_{n1}$ transition. For the overdamped modes, we used a coupling amounting to 50% of the ground state correlation function. For the $S^* \rightarrow S_n^*$ and $S_1 \rightarrow S_{n1}$ transitions, the same spectral density was used. These parameters result in a width of the transient absorption spectra that is in agreement with published data.[55] The difficulties to determine the spectral densities for the pathways that include population relaxation have further consequences. Since the strength of the ESA feature in the 2D spectra depends on the spectral density of the $S_1 \rightarrow S_{n1}/S^* \rightarrow S_n^*$ transition, it becomes difficult to determine the transition dipole moment of these transitions. As can be seen in Table 1, the transition dipole moments of the ESA transitions are rather large which could indicate that we have overestimated the reorganization energy of these transitions. Obtaining more detailed information about the spectral densities associated with the ESA transitions would thus help to reduce the uncertainty in the transition dipole moment of the ESA transition. We propose a three-pulse photon echo experiment directly on the $S_1 \rightarrow S_{n1}$ transition of the relaxed S_1 state to obtain a better estimation of this spectral density.

The pathways involving the $S_2 \rightarrow S_{n2}$ transition are associated with two spectral densities.[19,31] In the present study both are assumed to be identical and have the same temporal dependence

TABLE 2: Time Domain Parameters for the Spectral Densities of the Transitions Involved in the Model[a]

$\rho(S_0 \rightarrow S_2)$	τ (ps)	λ (cm^{-1})	ν (cm^{-1})
gauss	0.040	100	-
exp_1	0.15	300	-
exp_2	20	400	-
Vib_1	2.2	420	1150
Vib_2	2.2	1140	1520
$\rho(S_1 \rightarrow S_{n1})$	τ (ps)	λ (cm^{-1})	ν (cm^{-1})
gauss	0.040	50	-
exp_1	0.15	150	-
exp_2	20	200	-
Vib_1	0.2	72	1150
Vib_2	0.2	114	1520
Vib_3	0.2	135	1820

[a] In the table, τ denotes the characteristic time of the process, while λ denotes the reorganization energy of the specific mode. In the case of the vibrational modes τ denotes the dephasing time. The same spectral density was used for the $S_1 \rightarrow S_{n1}$ and $S^* \rightarrow S_n^*$ transition.

as the $S_0 \rightarrow S_2$ correlation function. The reorganization energy was set to 35% of the $S_0 \rightarrow S_2$ reorganization energy. To obtain more detailed information about this correlation function we propose a double quantum coherence experiment[61,62] that is capable of isolating the double coherence pathways particularly sensitive to these correlation functions. The details of the correlation functions of the $S_0 \rightarrow S_2$ and $S_1 \rightarrow S_{n1}/S^* \rightarrow S_n^*$ transitions used for the simulations are given in Table 2.

4.9. Pump−Deplete−Probe and the Nature of S*. The model presented in sections 4.1−4.8 can account for the observations of the 2D experiments as well as the essential features of the published pump−probe spectra. Having positioned S* as an excited state with branched decay from S_2, our model cannot account for the pump−deplete−probe experiments.[9,10] In these experiments, all pathways that are in S_2 population after the first two interactions (i.e., the pump pulse) are depleted via pumping of the NIR transition starting from S_2. It was shown that the depletion pulse only affected the S_1 part of the ESA signal, while the S* shoulder remained unchanged. On the basis of this finding, it was proposed that S* was a vibrationally hot ground state (see Figure 6, left panel). However, as discussed in section 4.3, it is not possible to construct a Feynman diagram in third order that has a negative sign if S* is positioned as a hot ground state, unless the hot ground state is populated via internal conversion from S_2. The ISRS process that was enlisted as the generating mechanism for the hot ground state will instead lead to a positive contribution in the 2D spectra. Even if two-photon interactions with the pump pulse are significant, there is a reported phenomenon the hot ground state hypothesis cannot account for. Niedzwiedzki et al.[23,24] reported that the S*-related spectral features lose amplitude upon freezing of the sample. The hot ground state should be unpopulated at ambient temperatures and hence not be affected by cooling of the sample. Concerning the origin of S*, it has been proposed that it is the result of a twisted conformation of the carotenoid.[23−25] It was argued that the lack of thermal energy in the low-temperature matrix prevented the excited-state twisting of the carotenoid and the formation of the S*. The main question in previous investigations is whether the conformational disorder is present in the ground state[24] or is formed after photoexcitation.[23] The inhibition of S* at low temperature gives no indication if the conformational change occurs in S_2 or S_0. If one assumes that the twisting occurs in S_2, this conformational change must be completed in

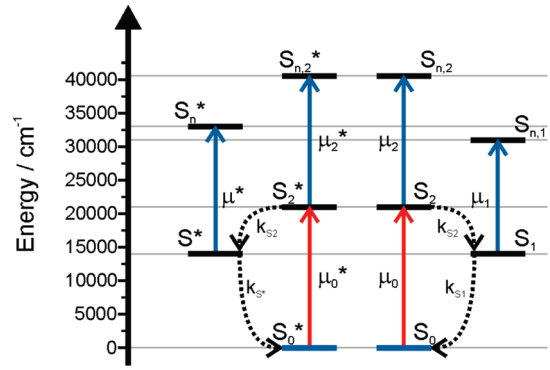

Figure 8. Model proposed to incorporate results from 2D, pump−probe at various temperatures and intensities, and pump−deplete−probe experiments. S* is the result of a conformation with its own set of energy levels (S_0, S_2, S_{n2}) denoted with a star.

150 fs to account for the observed rise of S*. Neglecting the complication of having such large scale nuclear motions on a 100 fs time scale, the main contradiction with the pump−deplete−probe experiments originates in the assumption that S* and S_1 are both formed by the same precursor state.

To resolve these difficulties in combining the results from the pump−deplete−probe experiment[9,10] and the intensity-dependent pump−probe measurements[21,22] with S* as an excited state, we propose that the two conformations exist already in the ground state[21,24] as shown in Figure 8. This hypothesis is supported by photon echo experiments[19] as well as the 2D experiments discussed above that have shown a significant inhomogeneous broadening that may be the result of conformational disorder. More direct evidence is given by recent results of Chábera et al.[63] They demonstrated that the GSB signal shows significantly more structure when S_1 has relaxed, compared to when both S_1 and S* contribute to the signal. This indicates that S* arises from a specific ground state conformation. If the properties of S* were determined only by the excited state properties, then the GSB would not change as the S_1 band relaxes, and only S* contributes to the signal. Interestingly, these results not only imply that the absorption band of carotenoids is heterogeneous but also show that the subpopulations corresponding to S_1 and S* couple to different spectral densities. Furthermore, no spectral shift was observed indicating that the two subconformations have similar vertical transition energies and only differ in the spectral shape of their absorption bands. Another similarity between S_1 and S* was revealed by Chábera et al.[63] by altering the polarity of the solvent. The position of the S* band was not affected by changing from benzene to DMSO. This indicates that S* is more likely to have A_g like S_1, rather than the ionic and hence solvent susceptible B_u symmetry. For benzonitrile, the polar solvent used in the experiment under discussion, this means that the conclusions drawn for S* can be directly related to less polar solvents.

If S_1 and S* are assumed to originate from different ground state conformations, it also becomes clear that they do not share a common S_2, and it becomes possible to account for the pump−deplete−probe experiment. It is clear that the $S^* \rightarrow S_n^*$ transition is shifted by almost 1000 cm^{-1} compared to the $S_1 \rightarrow S_{n1}$ transition in most systems.[9] It is thus not inconceivable that the NIR transition for different conformations may show a considerable spectral shift and may be missed by the depletion pulse. If the two conformers both show a transient absorption signal in the NIR region, we expect the transition to be spectrally heterogeneous. The spectral evolution of the NIR transient absorption spectra does, in fact, display two components with

different kinetics.[49] The two distinct spectral components could be the result of the spectral shift between the NIR transition of the two conformational distributions discussed above. Further support for the idea that different conformations may have significantly shifted NIR transitions can be found in the work of Niedzwiedzki et al.[50] showing a spectral shift of hundreds of cm^{-1} between the geometrical isomers of various carotenoids in the NIR region for transitions originating from S_2. Not only the spectral shift between the NIR transitions of the different conformational subpopulations may affect the inability to bleach the S* contribution but also the magnitude of the S_2-transition dipole moment in the NIR may significantly change after a twist of the backbone. For the geometric isomers,[50] the change of the transition dipole moment in the NIR region is approximately a factor of 2.[64]

We propose that S* is associated with S_1 of a twisted conformation of the carotenoid. This twisted conformation is not produced in the relaxation from S_2 but rather is present already in the ground state. The conformation does not only affect the ground state but also leads to a shift of the transition energy of all electronic transitions. A more complete picture of the carotenoid electronic structure would thus have a double set of electronic levels, (S_0, S_{0*}), (S_1, S*), (S_2, S_2*), and (S_{n2}, S_{n2}*) as shown in Figure 8. We argue that the inability to bleach the S* spectral feature in the pump−deplete−probe experiment has its origin in a spectral shift of the NIR transition of the S* conformation, possibly combined with a weaker transition dipole moment. The model in Figure 8 can also account for the intensity-dependent studies[21,22] since it incorporates both inhomogeneity as well as the additional $S_2 \rightarrow S_{n2}$ transition, effectively being a mixture between the inhomogenous and the two-photon model discussed by Papagiannakis et al.[21] From our discussion, it is clear that future research on carotenoid photophysics should focus on the influence of conformational changes on the electronic structure. It is unlikely that numerical simulations based on the model in Figure 8 would lead to new insights since adding the inhomogeneous distribution will inevitably lead to the introduction of many new parameters that are difficult to estimate from experiments. Rather, we propose that the model in Figure 8 can be verified by investigations of the transient absorption spectra in the NIR region at low temperature to see if the disappearance of S* in the visible region[23,24] is correlated to spectral changes in the transition from S_2.

5. Conclusions

2D electronic spectroscopy has been used to investigate the spectrally congested red edge of β-carotene's linear absorption spectrum. The ability of 2D to lift spectral congestion has allowed a novel perspective on the spectral region where GSB, SE, and ESA overlap. We find no spectral signature of any intermediate state between S_2 and S_1 in the 2D spectra despite the ability of 2D to highlight such features via cross peaks. An analysis of the Feynman diagrams in third order show that S* needs to be an excited electronic state to account for the experimental observations in 2D and pump−probe. Furthermore, the 2D results demonstrate that S* exhibits rise kinetics similar to S_1. Since we can rule out signal contributions from $\chi^{(5)}$-terms for the employed excitation densities, we exclude a vibrationally hot ground state as the origin of S*. Hence, an analysis of the relevant $\chi^{(3)}$-Feynman diagrams together with the observation of ESA from S_2 covered by the GSB are strong arguments for the two-photon model proposed by Papagiannakis et al.[21] However, since this model is not able to account for the pump−deplete−probe experiment, it is clear that the final model of β-carotene's photophysics must also include ground state inhomogeneity. We have proposed that S* is the result of a twisted conformation of the carotenoid already present in the ground state. The explanation for the pump−deplete−probe experiment is in this model related to the different spectral position and strength of the NIR transition of the subpopulations responsible for S* and S_1. Hence, electronic 2D in combination with modeling enables a comprehensive, insightful, and experimentally well-founded perspective on intricate molecular photodynamics. This wealth of spectroscopic information is unattainable via lower-dimensional signals like, e.g., pump−probe techniques.

Acknowledgment. N.C. acknowledges financial support from European Science Foundation (ESF) within the Ultrafast Structural Dynamics in Physics, Chemistry, Biology and Material Science (DYNA) program. Work in Lund is financed by the Swedish Research Council and KAW foundation. J.H. would like to thank the FWF Austrian Science Fund for financial support by a Lise-Meitner scholarship. A.N. and J.S. thank the Austrian Academy of Sciences for financial support by the doctoral scholarship program (DOC-fFORTE and DOC). All authors appreciate helpful discussions with T. Polivka from the University of South Bohemia, with T. Buckup from the University of Marburg, and with H. A. Frank from the University of Connecticut.

References and Notes

(1) Polivka, T.; Sundstrom, V. *Chem. Rev.* **2004**, *104*, 2021.
(2) Wasielewski, M. R.; Kispert, L. D. *Chem. Phys. Lett.* **1986**, *128*, 238.
(3) Polivka, T.; Sundstrom, V. *Chem. Phys. Lett.* **2009**, *477*, 1.
(4) Frank, H. A. *Arch. Biochem. Biophys.* **2001**, *385*, 53.
(5) Ricci, M.; Bradforth, S. E.; Jimenez, R.; Fleming, G. R. *Chem. Phys. Lett.* **1996**, *259*, 381.
(6) Macpherson, A. N.; Gillbro, T. *J. Phys. Chem. A* **1998**, *102*, 5049.
(7) Fujiwara, M.; Yamauchi, K.; Sugisaki, M.; Gall, A.; Robert, B.; Cogdell, R. J.; Hashimoto, H. *Phys. Rev. B* **2008**, *77*, 205118.
(8) Sugisaki, M.; Yanagi, K.; Cogdell, R. J.; Hashimoto, H. *Phys. Rev. B* **2007**, *75*.
(9) Buckup, T.; Savolainen, J.; Wohlleben, W.; Herek, J. L.; Hashimoto, H.; Correia, R. R. B.; Motzkus, M. *J. Chem. Phys.* **2006**, *125*, 194505.
(10) Wohlleben, W.; Buckup, T.; Hashimoto, H.; Cogdell, R. J.; Herek, J. L.; Motzkus, M. *J. Phys. Chem. B* **2004**, *108*, 3320.
(11) Hauer, J.; Buckup, T.; Motzkus, M. *J. Phys. Chem. A* **2007**, *111*, 10517.
(12) Hornung, T.; Skenderovic, H.; Motzkus, M. *Chem. Phys. Lett.* **2005**, *402*, 283.
(13) Kukura, P.; McCamant, D. W.; Mathies, R. A. *J. Phys. Chem. A* **2004**, *108*, 5921.
(14) McCamant, D. W.; Kukura, P.; Mathies, R. A. *J. Phys. Chem. A* **2003**, *107*, 8208.
(15) McCamant, D. W.; Kukura, P.; Yoon, S.; Mathies, R. A. *Rev. Sci. Instrum.* **2004**, *75*, 4971.
(16) Buckup, T.; Lebold, T.; Weigel, A.; Wohlleben, W.; Motzkus, M. *J. Photochem. Photobiol. A-Chem.* **2006**, *180*, 314.
(17) Hauer, J.; Buckup, T.; Motzkus, M. *Chem. Phys.* **2008**, *350*, 220.
(18) Savolainen, J.; Fanciulli, R.; Dijkhuizen, N.; Moore, A. L.; Hauer, J.; Buckup, T.; Motzkus, M.; Herek, J. L. *Proc. Natl. Acad. Sci. U.S.A.* **2008**, *105*, 7641.
(19) Christensson, N.; Polivka, T.; Yartsev, A.; Pullerits, T. *Phys. Rev. B* **2009**, *79*, 24–245118.
(20) Gradinaru, C. C.; Kennis, J. T. M.; Papagiannakis, E.; van Stokkum, I. H. M.; Cogdell, R. J.; Fleming, G. R.; Niederman, R. A.; van Grondelle, R. *Proc. Natl. Acad. Sci. U.S.A.* **2001**, *98*, 2364.
(21) Papagiannakis, E.; van Stokkum, I. H. M.; Vengris, M.; Cogdell, R. J.; van Grondelle, R.; Larsen, D. S. *J. Phys. Chem. B* **2006**, *110*, 5727.
(22) Savolainen, J.; Buckup, T.; Hauer, J.; Jafarpour, A.; Serrat, C.; Motzkus, M.; Herek, J. L. *Chem. Phys.* **2009**, *357*, 181.
(23) Niedzwiedzki, D.; Koscielecki, J. F.; Cong, H.; Sullivan, J. O.; Gibson, G. N.; Birge, R. R.; Frank, H. A. *J. Phys. Chem. B* **2007**, *111*, 5984.
(24) Cong, H.; Niedzwiedzki, D. M.; Gibson, G. N.; Frank, H. A. *J. Phys. Chem. B* **2008**, *112*, 3558.

(25) Niedzwiedzki, D. M.; Sullivan, J. O.; Polivka, T.; Birge, R. R.; Frank, H. A. *J. Phys. Chem. B* **2006**, *110*, 22872.
(26) Cervetto, V.; Helbing, J.; Bredenbeck, J.; Hamm, P. *J. Chem. Phys.* **2004**, *121*, 5935.
(27) Cho, M. H. *Chem. Rev.* **2008**, *108*, 1331.
(28) Jonas, D. M. *Annu. Rev. Phys. Chem.* **2003**, *54*, 425.
(29) Joo, T. H.; Jia, Y. W.; Yu, J. Y.; Lang, M. J.; Fleming, G. R. *J. Chem. Phys.* **1996**, *104*, 6089.
(30) Lepetit, L.; Joffre, M. *Opt. Lett.* **1996**, *21*, 564.
(31) Brixner, T.; Mancal, T.; Stiopkin, I. V.; Fleming, G. R. *J. Chem. Phys.* **2004**, *121*, 4221.
(32) Mukamel, S. *Principles of Non-linear Optical Spectroscopy*; Oxford University Press: New York, 1995.
(33) Roberts, S. T.; Loparo, J. J.; Tokmakoff, A. *J. Chem. Phys.* **2006**, *125*, 084502.
(34) Brixner, T.; Stiopkin, I. V.; Fleming, G. R. *Opt. Lett.* **2004**, *29*, 884.
(35) Cowan, M. L.; Ogilvie, J. P.; Miller, R. J. D. *Chem. Phys. Lett.* **2004**, *386*, 184.
(36) Riedle, E.; Beutter, M.; Lochbrunner, S.; Piel, J.; Schenkl, S.; Sporlein, S.; Zinth, W. *Appl. Phys. B* **2000**, *71*, 457.
(37) Nemeth, A.; Milota, F.; Mancal, T.; Lukes, V.; Kauffmann, H. F.; Sperling, J. *Chem. Phys. Lett.* **2008**, *459*, 94.
(38) Milota, F.; Sperling, J.; Nemeth, A.; Kauffmann, H. F. *Chem. Phys.* **2009**, *357*, 45.
(39) Tauber, M. J.; Mathies, R. A.; Chen, X. Y.; Bradforth, S. E. *Rev. Sci. Instrum.* **2003**, *74*, 4958.
(40) Koyama, Y.; Takatsuka, I.; Nakata, M.; Tasumi, M. *J. Raman Spectrosc.* **1988**, *19*, 37.
(41) Lazonder, K.; Pshenichnikov, M. S.; Wiersma, D. A. *Opt. Lett.* **2006**, *31*, 3354.
(42) Billsten, H. H.; Zigmantas, D.; Sundstrom, V.; Polivka, T. *Chem. Phys. Lett.* **2002**, *355*, 465.
(43) Buckup, T.; Hauer, J.; Mohring, J.; Motzkus, M. *Arch. Biochem. Biophys.* **2009**, *483*, 219.
(44) Stenger, J.; Madsen, D.; Hamm, P.; Nibbering, E. T. J.; Elsaesser, T. *J. Phys. Chem. A* **2002**, *106*, 2341.
(45) Hauer, J.; Skenderovic, H.; Kompa, K. L.; Motzkus, M. *Chem. Phys. Lett.* **2006**, *421*, 523.
(46) Xu, Q. H.; Ma, Y. Z.; Stiopkin, I. V.; Fleming, G. R. *J. Chem. Phys.* **2002**, *116*, 9333.
(47) Cerullo, G.; Polli, D.; Lanzani, G.; De Silvestri, S.; Hashimoto, H.; Cogdell, R. J. *Science* **2002**, *298*, 2395.
(48) Kosumi, D.; Komukai, M.; Hashimoto, H.; Yoshizawa, M. *Phys. Rev. Lett.* **2005**, *95*, 213601.
(49) Zhang, J. P.; Skibsted, L. H.; Fujii, R.; Koyama, Y. *Photochem. Photobiol.* **2001**, *73*, 219.
(50) Niedzwiedzki, D. M.; Sandberg, D. J.; Cong, H.; Sandberg, M. N.; Gibson, G. N.; Birge, R. R.; Frank, H. A. *Chem. Phys.* **2009**, *357*, 4.
(51) Andersson, P. O.; Gillbro, T. *J. Chem. Phys.* **1995**, *103*, 2509.
(52) Kosumi, D.; Fujiwara, M.; Fujii, R.; Cogdell, R. J.; Hashimoto, H.; Yoshizawa, M. *J. Chem. Phys.* **2009**, *130*, 214506.
(53) Kosumi, D.; Yanagi, K.; Fujii, R.; Hashimoto, H.; Yoshizawa, M. *Chem. Phys. Lett.* **2006**, *425*, 66.
(54) Polli, D.; Cerullo, G.; Lanzani, G.; De Silvestri, S.; Yanagi, K.; Hashimoto, H.; Cogdell, R. J. *Phys. Rev. Lett.* **2004**, *93*, 163002.
(55) Lustres, J. L. P.; Dobryakov, A. L.; Holzwarth, A.; Veiga, M. *Angew. Chem., Int. Ed.* **2007**, *46*, 3758.
(56) Englman, R.; Jortner, J. *Mol. Phys.* **1970**, *18*, 145.
(57) Nitzan, A.; Mukamel, S.; Jortner, J. *J. Chem. Phys.* **1975**, *63*, 200.
(58) Fuss, W.; Haas, Y.; Zilberg, S. *Chem. Phys.* **2000**, *259*, 273.
(59) Garavelli, M.; Celani, P.; Bernardi, F.; Robb, M. A.; Olivucci, M. *J. Am. Chem. Soc.* **1997**, *119*, 11487.
(60) Christensen, R. L.; Goyette, M.; Gallagher, L.; Duncan, J.; DeCoster, B.; Lugtenburg, J.; Jansen, F. J.; van der Hoef, I. *J. Phys. Chem. A* **1999**, *103*, 2399.
(61) Abramavicius, D.; Voronine, D. V.; Mukamel, S. *Proc. Natl. Acad. Sci. U.S.A.* **2008**, *105*, 8525.
(62) Kim, J.; Mukamel, S.; Scholes, G. D. *Acc. Chem. Res.* **2009**, *42*, 1375.
(63) Chabera, P.; Fuciman, P.; Hribek, P.; Polivka, T. *Phys. Chem. Chem. Phys.* **2009**, *11*, 8795.
(64) Frank, H. A., personal communication.

JP906604J